Using Directed Self Assembly of Block Copolymer Nanostructures to Modulate Nanoscale Surface Roughness: Towards a Novel Lithographic Process

*Ya-Mi Chuang, Kevin S. Jack, Han-Hao Cheng, Andrew K. Whittaker, and Idriss Blakey**

Nanoscale surface roughness is an important factor in determining the properties of surfaces and can affect the performance of a range of devices prepared by lithographic methods. Here, a method is reported, which enables modulation of the nanoscale roughness of surfaces through the directed self assembly (DSA) of positively charged polymersomes, composed of specifically designed block copolymers, onto negatively charged surfaces. Assembly of the polymersomes on surfaces can result in an increase in the nanoscale surface roughness; however, through a controlled annealing step we can also significantly reduce the nanoscale roughness of the original surface. The ability to decrease the roughness of lithographic patterns is expected to have a significant impact on the manufacture of integrated circuits.

1. Introduction

Surface topography at the nanoscale has the potential to impact on many important material properties.[1,2] For example, rough surfaces can exhibit decreased adhesion,[3] friction[4] and gloss when compared to their flat counterparts.[5] On the other hand, the hydrophobicity of a material tends to increase with increasing roughness, where certain topographies can result in superhydrophobicity, even for materials that would normally be hydrophilic when smooth.[6] Consequently, nanoscale roughness can affect the performance of different devices, which include biomaterials,[7–11] micro-/nano-electromechanical systems (M/NEMS)[12,13] and microelectronics.[14,15] The issue of roughness is of particular concern in the manufacture of advanced microelectronics, where the feature sizes of transistor components are currently as small as 32 nm and will likely reduce to 22 and 16 nm in the coming years.[16] The inherent roughness of printed features, commonly termed line-edge roughness (LER) or line-width roughness (LWR), is predicted to significantly degrade device performance at these small feature sizes. For example, low-frequency roughness can induce variations in transistor speed, because this affects the transport of electrons.[17,18] On the other hand, high-frequency roughness can cause local variations in voltage, which may affect the current leakage, or the threshold voltages of transistors.[19,20] Despite many studies into mediating this phenomenon there is currently no process or material that can reduce LER to the targets set by the semiconductor industry.[21–26]

Directed self assembly of block copolymers is a method of interest for generating regular patterns with nanosized dimensions that are much smaller than can be printed with conventional lithography techniques,[27–30] such that density multiplication of printed features is possible.[31–46] Directed self assembly has also been used for the repair[47] and shrinking of the critical dimensions[48] of lithographically printed features. In this paper we report the use of a process that can be used to either induce roughness in a smooth surface, or smooth rough surfaces to the nanometer level. The process involves the directed self assembly of charged polymeric vesicles, composed of block copolymers, on surfaces through electrostatic attraction, which results in roughening of smooth surfaces. By undertaking an annealing step, which alone does not affect the morphology of the substrate, it is possible to tune the magnitude of the surface roughness. The process is made possible by careful selection of the respective blocks in the block copolymers that make up the polymeric vesicles, such that the blocks are glassy at room temperature, but can undergo structural reorganization at elevated temperatures where the photoresist substrates typically used in lithography remain rigid. When this methodology is applied to rough surfaces it is possible to significantly reduce surface roughness. Hence, the general process may be applicable to smoothing of lithographically prepared features or to applications that require a degree of roughness to be induced without mechanical abrasion or chemical etching.

2. Results and Discussion

Scheme 1 summarizes the general procedure used in this study to modify the roughness of surfaces. Amphiphilic

Y.-M. Chuang, Dr. H.-H. Cheng, Prof. A. K. Whittaker, Prof. I. Blakey
The University of Queensland
Centre for Advanced Imaging and Australian Institute for Bioengineering and Nanotechnology
St Lucia, Queensland, 4072 Australia
E-mail: i.blakey@uq.edu.au
Dr. K. S. Jack
The University of Queensland
Centre for Microscopy and Microanalysis
St Lucia, Queensland, 4072 Australia

DOI: 10.1002/adfm.201200564

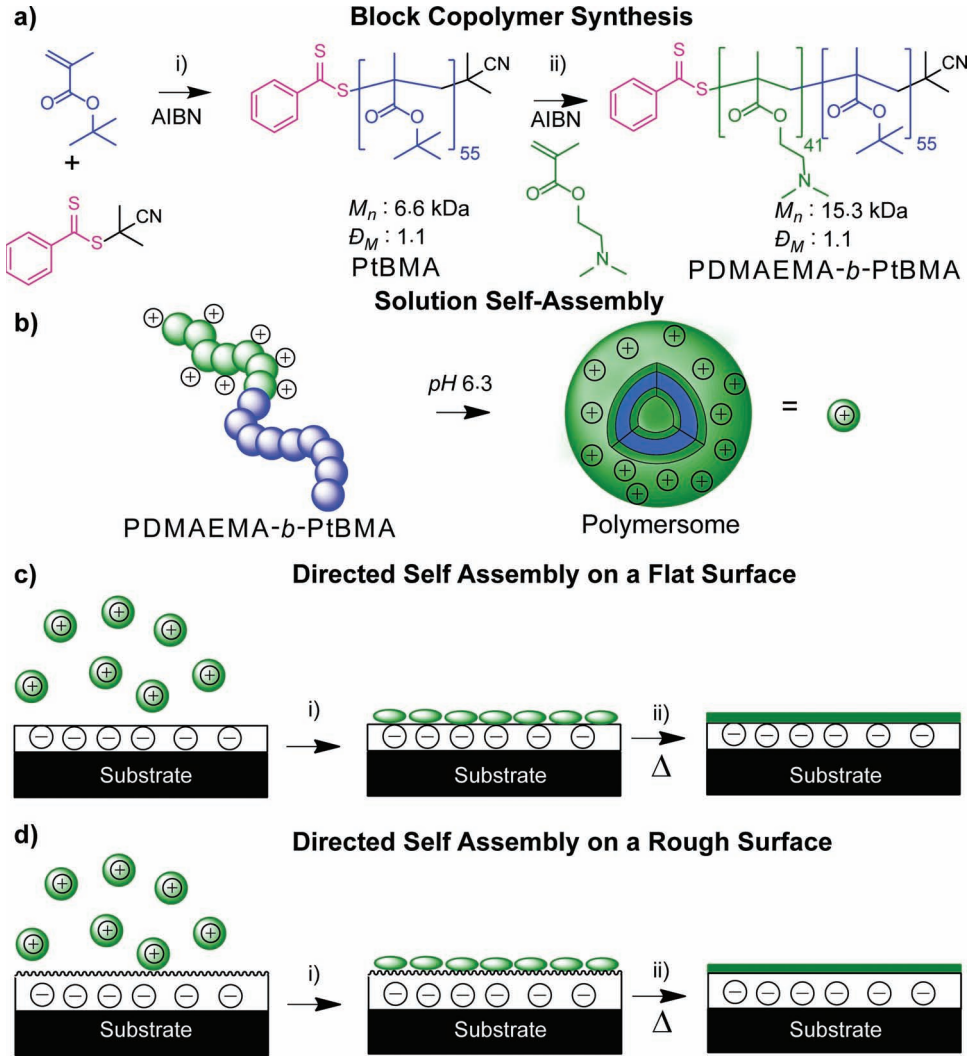

Scheme 1. a) i) Preparation of PtBMA via RAFT mediated polymerization; ii) Chain extension of PtBMA macroinitiator with DMAEMA. b) Self assembly of PDMAEMA-*block*-PtBMA into polymersomes. c) i) Modification of model, flat, negatively charged surfaces with positively charged polymersomes; ii) Annealing of surfaces to tune roughness. d) i) Modification of model, rough, negatively charged surfaces with positively charged polymersomes; ii) Annealing of surfaces to heal roughness. The diagrams are not drawn to scale.

block copolymers were prepared using controlled radical polymerization (Scheme 1a) and assembled into polymersomes that carry a residual positive charge in acidic aqueous solutions(Scheme 1b). The polymersomes were deposited onto negatively charged surfaces, which were either flat (Scheme 1c) or rough (Scheme 1d). These coated surfaces were then annealed at a range of temperatures to control the final nanoscale roughness.

2.1. Synthesis of Block Copolymers

We have synthesized well-defined poly(2-(*N*,*N*-dimethylamino)ethyl methacrylate)-*block*-poly(*tert*-butyl methacrylate) (PDMAEMA-*block*-PtBMA) using reversible addition-fragmentation chain-transfer (RAFT) polymerization.[49,50] RAFT polymerization allows synthesis of polymers with a range of architectures such as linear, block,[51–53] star[51,52,54] and branched polymers[55,56] with controlled molar mass and low molar-mass dispersity ($Đ_M$). This polymerization method also has significant versatility in terms of functional group tolerance.[57]

The first step in preparation of the block copolymer involved the synthesis of the PtBMA block and from size exclusion chromatography (SEC) the number-average molecular weight (M_n) was found to be 6.6 kDa relative to polystyrene standards, with a $Đ_M$ of 1.1. The PtBMA macroinitiator was subsequently chain extended with DMAEMA to give a diblock copolymer with a M_n of 15.3 kDa and a $Đ_M$ of 1.1. The SEC results are presented in **Figure 1**a, and show the progression to higher molecular weight after chain extension. This polymer was fully characterized by ^{1}H NMR, ^{13}C NMR, and FTIR spectroscopy, DSC, and thermogravimetric analysis (TGA) (see Supporting Information) and these data were consistent with successful

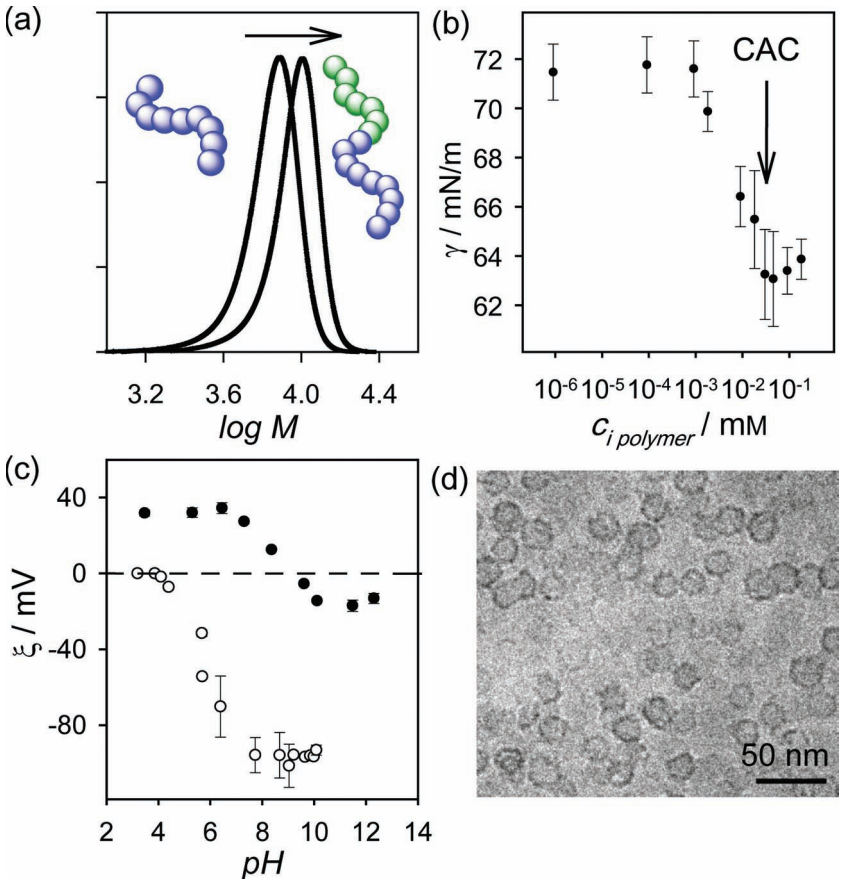

Figure 1. a) SEC chromatograms showing molecular-weight distribution of PtBMA (left) and the successful chain extension with DMAEMA (right). b) Interfacial tension, γ, of aqueous solutions of the block copolymer as a function of polymer concentration, $c_{i\ polymer}$, at pH 6.3. c) Zeta potential, ζ, of PDMAEMA$_{41}$-*block*-PtBMA$_{55}$ in 10 mM NaCl$_{(aq.)}$ at pH values ranging from 3.2–12.5 (solid dots); and of films of the PtBMA$_{0.42}$-*stat*-PMMA$_{0.56}$-*stat*-PGMA$_{0.02}$ at pH values ranging from 3.2–10.2 (open dots). d) Cryo-TEM micrograph of 0.6 mg/mL of PDMAEMA$_{41}$-*block*-PtBMA$_{55}$ at pH 6.3. Many spherical particles with higher electron density at the shell (dark contrast) are observed, indicating the formation of polymersomes.

formation of the block copolymer. PDMAEMA was selected as one of the blocks due to its ability to carry positive charges when the polymer is dissolved in aqueous solutions that have pH values less than 8.[58,59] From DSC measurements, a single glass transition temperature (T_g) of PDMAEMA$_{41}$-*block*-PtBMA$_{55}$ was observed at 67 °C. According to literature, PDMAEMA and PtBMA have glass transition temperatures of 25 °C and 88.5 °C, respectively.[59,60] The glass T_g as a function of composition, degree of polymerization and the blockiness can be predicted from the Barton–Johnston equation.[61] For the PDMAEMA-*block*-PtBMA reported here it was predicted to be approximately 61 °C, which is similar to the value measured by DSC. Most importantly, this temperature is below the T_g of the substrates to be modified in subsequent steps; which are typically >120 °C. The ability to control the T_g of the modifying block copolymer, through judicious of polymers, is especially important in lithographic applications where annealing steps at above the T_g of the photoresist would result in reflow or collapse of the patterned features.

2.2. Block Copolymer Self Assembly

The block copolymer PDMAEMA$_{41}$-*block*-PtBMA$_{55}$ is amphiphilic in nature, and so is expected to undergo self assembly in aqueous solution. The critical aggregation concentration (CAC) was assessed by monitoring the surface tension, γ, of polymer solutions as a function of concentration (Figure 1b). As can be seen from this figure, below a concentration of 9×10^{-4} mM the surface tension was approximately 71 mN/m, while between 9×10^{-4} and 3×10^{-2} mM the surface tension dropped to about 63 mN/m with increasing concentration and reached a plateau value at concentrations greater than 3×10^{-2} mM. The CAC was thus estimated to be 3×10^{-2} mM. For the surface modification experiments described later in this report we used polymer concentrations that are much greater than the CAC.

The surface charges of the particles formed above the CAC were determined from measurements of zeta potential, ζ, as a function of pH and are shown in Figure 1c. Below a pH of approximately 6.3 the charge of the particles was constant, at ca. +35 mV, while for pH values from 7.8 to 10 the charge steadily decreased to about –20 mV with increasing pH. In this study we are interested in well dispersed structures with a net positive charge, so in subsequent experiments we have used solutions of the block copolymers having pH values of 6.3 or less.

To understand the morphology of the particles in solution, cryogenic transmission electron microscopy (cryo-TEM) was carried out. Figure 1d shows a cryo-TEM image of a 0.04 mM aqueous solution of PDMAEMA$_{41}$-*block*-PtBMA$_{55}$ at pH 6.3. The contrast observed in the TEM image arises from the difference in the electron density within the material, where bright regions have low electron density and dark regions have high electron density. A number of spherical particles can be observed. These particles have an average diameter of 18 ± 2 nm and the shell (dark contrast) has a thickness of approximately 4 nm and center of the particles has bright contrast indicating that they are hollow. The block copolymer is made up of a hydrophilic block, which makes up 46% by volume. The packing parameter (p) of the block copolymer was determined to be 0.5, which is within the range suggested for formation of polymersomes.[62,63] and in conjunction with the observed cryo-TEM images it is concluded that the block copolymers form polymersomes at pH 6.3.

2.3. Directed Self Assembly onto Negatively Charged, Flat Surfaces

A targeted application of this work is the healing of nanoscale roughness of features that have been printed using

photolithography. The chemical changes that occur in conventional photoresists as a result of irradiation and annealing involve deprotection of hydrophobic esters into hydrophilic carboxylic acids and this strategy is commonly used in a range of different lithography platforms (e.g., 248 nm,[64] 193 nm,[64] and extreme ultraviolet lithography (EUVL).[65]) This switch in solubility allows the regions irradiated with light to be selectively removed by dissolution with an aqueous base. At the boundary of the exposed and unexposed polymer, however, there resides an interphase region consisting of partially deprotected polymer chains, which imparts a high negative charge to the side-walls of the patterned features.[66] This negative charge will be used to direct the self assembly of the positively charged polymersomes, with the intention of ultimately smoothing the nanoscale surface roughness of the side walls. However, to understand this process we initially require a model flat surface. Substrates such as glass or certain polymers (e.g., poly(methyl methacrylate) (PMMA)) have an inherent negative surface charge.[67] However, the density of charge at the surface of these materials within our proposed working range of pH values for deposition of the polymersomes was found to be insufficient to achieve good coverage of polymersomes. For example, treatment of a thin film of PMMA with solutions of the polymersome resulted in 53% coverage of the colloids (see Supporting Information, Figure S9). This is due to PMMA being reported to have a surface charge of only –12 mV at pH 6.3.[67] For this reason it was necessary for us to fabricate smooth surfaces that were more negatively charged.

The method used to produce negatively-charged smooth surfaces is analogous to that reported by others for tuning the surface energy of substrates.[68,69] However, we have modified these procedures by using polymers that have some repeat units that contain pendant tertiary esters, which during processing undergo deprotection to form carboxylic acids and, therefore, can impart a negative charge under appropriate conditions. Briefly, a statistical copolymer of tertiary butyl methacrylate, methyl methacrylate and glycidyl methacrylate (PtBMA$_{0.42}$-*stat*-MMA$_{0.56}$-*stat*-GMA)$_{0.02}$) in a solution containing 5 wt% of a photoacid generator (PAG) (with respect to the copolymer content) was spin-coated onto a silicon wafer. The resultant thin film (19.8 ± 0.6 nm) was then irradiated with UV light to induce photodecomposition of the PAG, thus generating a strong acid. During the subsequent annealing step carried out at 150 °C, the strong acid catalyses the crosslinking of the epoxide groups to stabilize the film. Annealing in the presence of a strong acid also resulted in deprotection of the tertiary esters to give carboxylic acids. Following washing with a range of solvents, such as propylene glycol methyl ether acetate (a good solvent for the starting polymer) and water (a good solvent for uncrosslinked hydrophilic polymer) it was found through ellipsometry that the film thickness did not change significantly, thus confirming effective crosslinking. The formation of carboxylic acids was also confirmed using grazing angle attenuated total reflectance FTIR spectroscopy (see Supporting Information, Figure S10). The carboxylic acids formed during the process are expected to impart a larger negative charge when exposed to solutions with moderate to high pH values. Streaming potential measurements were used to determine the zeta potential of the surface as a function of pH (see Figure 1c). Below a pH of 4 the surface carries virtually no charge, while above this pH the surface becomes negatively charged. At pH 6.3 it was found that the charge of the surface was –63 mV. Therefore, working at a pH of 6.3 should ensure that the positively charged polymersomes will bind to the negatively charged surface.

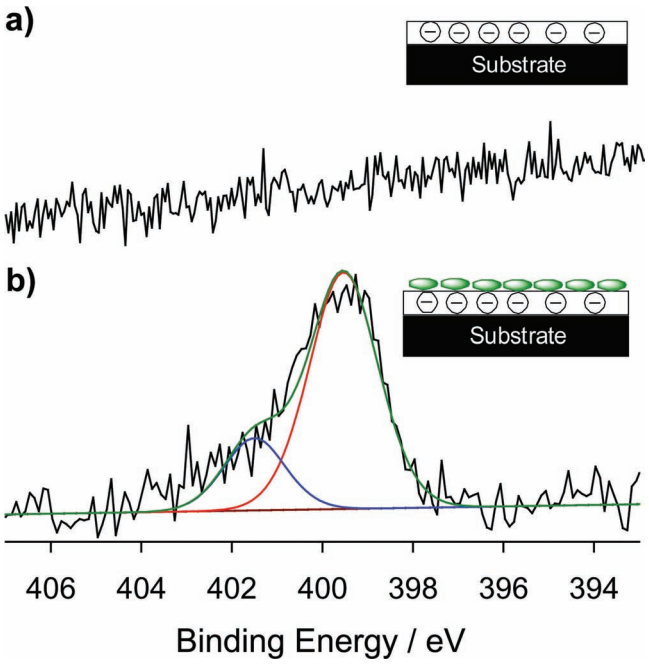

Figure 2. Stacked high-resolution SXPS spectra of the model negatively charged surface before (a) and after (b) deposition of the polymersomes (black lines). The N1s peak appears in (b) after it has been dip-coated and rinsed, and is evidence of electrostatic attraction between the polymersomes and the negatively charged surface. Curve fitting of the charged (blue line) and uncharged (red line) species at 402 and 399 eV, respectively, are also shown. The total fitted curve is shown in green.

In order to study the interaction of the polymersomes with this negatively charged model surface, it was dip coated in an aqueous solution of the polymersomes. The thicknesses of the polymer coating before and after treatment with polymersomes were measured using ellipsometry and were observed to slightly increase from 19.8 ± 0.6 nm to 21.8 ± 0.4 nm. This small increase, compared with the observed diameter of the polymersomes, which was 18.5 nm by TEM, suggests that the polymersomes do not retain their spherical morphology after attachment and drying. To further investigate this, the surfaces were analyzed using synchrotron X-ray photoelectron spectroscopy (SXPS) and atomic force microscopy (AFM). SXPS was used due to the low relative sensitivity factor of nitrogen, which can be difficult to detect and quantify using a laboratory XPS. **Figure 2**a,b show high-resolution SXPS spectra in the N1s region before and after treatment with the polymersomes, respectively. Prior to treatment no significant nitrogen peak was observed, while after treatment with the block copolymer solution, peaks at 399 and 402 eV are clearly evident, which arise from the nitrogen-containing PDMAEMA block and confirm the adherence of the block copolymer to the model surface. The peak at 399 eV is assigned to uncharged nitrogen atoms, while the peak at 402 eV is assigned to charged nitrogen atoms.[70] Curve

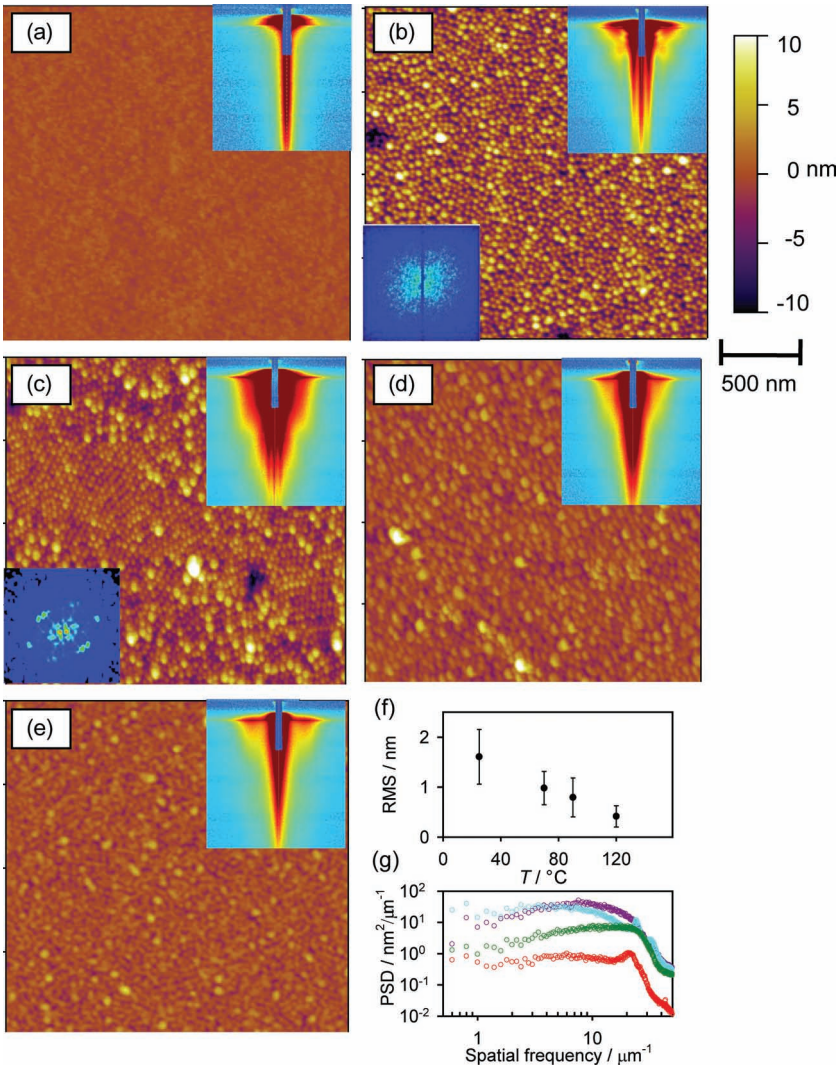

Figure 3. a–e) AFM images showing the topology of a negatively charge flat surface (a), and after coating with polymersomes and annealing at room temperature (b), 70 °C (c), 90 °C (d) and 120 °C (e) for 6 minutes. The top-right inset in the AFM images shows the corresponding 2D GISAXS patterns of the surfaces, while the bottom-left insets for (b) and (c) are the fast Fourier transforms of the AFM images. f) The RMS surface-roughness values determined by AFM after annealing at various temperatures. g) PSD analysis for a negatively charged surface after treatment with polymersomes (purple circles), after annealing to 70 °C (cyan circles), after annealing at 90 °C (green circles) and after annealing to 115 °C (red circles).

fitting of this region revealed that there was 79% uncharged and 21% charged nitrogen atoms. In our system the charge of the polymersomes in aqueous solution is controlled by addition of HCl. We believe the observation of mainly uncharged species is due to desorption of HCl in the high vacuum environment of the SXPS analysis chamber. Nonetheless, the observation of nitrogen peaks following treatment of the surface, provides spectroscopic evidence that the positively charged polymersomes are adhering onto the negatively charged surface.

The morphology of a negatively charged surface before and after treatment with the solution of polymersomes was studied using AFM and the images are shown in **Figure 3**. The false-color height images show the surfaces before treatment (Figure 3a), after exposure to the solution of polymersomes (Figure 3b) and after annealing at different temperatures (Figure 3c–e). The virgin, crosslinked $PtBMA_{0.42}$-*stat*-$MMA_{0.56}$-*stat*-$GMA)_{0.02}$ was found to have a root mean square (RMS) roughness of 0.3 ± 0.2 nm (see Figure 3f), which is marginally rougher than the uncoated silicon wafer substrate. After treatment with a solution of the polymersomes (0.6 mg/mL $PDMAEMA_{41}$-*block*-$PtBMA_{55}$ at pH 6.3) a large number of spherical structures with an average diameter of 46 ± 2 nm can be observed (Figure 3b) and image analysis indicates that the coverage is approximately 99%. The increased size of the particles compared to that observed via cryo-TEM (18.5 ± 1.8 nm) is consistent with flattening of the polymersomes during the deposition and drying steps. It should also be noted that the RMS roughness of the film was found to increase to 1.6 ± 0.6 nm after deposition of the polymersomes.

An annealing temperature of 70 °C was initially selected, because it was higher than the measured T_g for the block copolymer and from Figure 3c it can qualitatively be seen that after annealing at 70 °C for four minutes some increase in ordering of the particles on the surface is evident. To further highlight the increase in ordering upon annealing at 70 °C, Fourier transforms of the 2D radial distribution function are shown as insets in the bottom left hand corners of Figure 3b,c, with the latter showing evidence of mixed hexagonal and cubic packing.[71] Increasing the temperature, however, results in the spherical structures becoming less distinct and the RMS roughness steadily decreases to 0.4 ± 0.2 nm for the samples annealed to 120 °C. This demonstrates that the nanoscale roughness can be tuned by using different annealing temperatures. To better understand how the PSD varies with the spatial frequency, the AFM images for samples at each stage of annealing have also undergone power spectral density (PSD) analysis (Figure 3g). After heating to 70 °C, there is a small drop in PSD between 10–20 μm^{-1} and peaks appear at 23 and 30 μm^{-1}, which corresponds to 43 and 33 nm respectively. These peaks are consistent with ordering of the polymersomes. Upon heating to 90 °C the peaks disappear and the PSD at greater than 20 μm^{-1} decreases significantly. Upon heating to 120 °C significant decreases over the entire spatial frequency range were observed.

This annealing process was also investigated by grazing-incidence small-angle scattering (GISAXS), and the 2D scattering images are shown as insets in the top right-hand corner of the AFM images in Figure 3. It should be noted that the GISAXS is only providing information in the x–y plane and no information regarding the structure in the z plane was obtained in this experiment. The as-deposited polymersomes

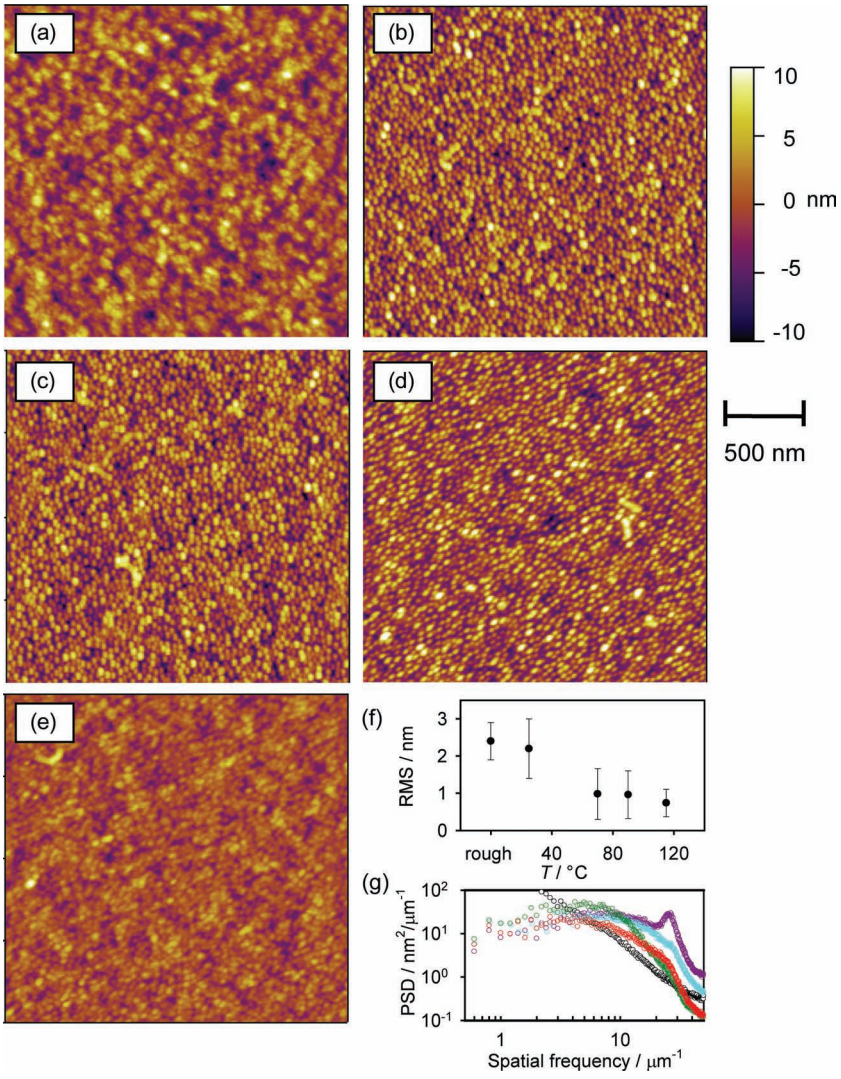

Figure 4. a–e) AFM images showing the topology of the model, rough surface (a), after coating with polymersomes room temperature annealing (b), and after annealing at 70 °C (c), 90 °C (d) and 115 °C (e) for 6 minutes. f) A plot of RMS values determined by AFM as a function of annealing temperature for the model, rough surfaces treated with the polymersomes. g) PSD analysis for a model, rough surface (black circles), after treatment with polymersomes (purple circles), after annealing to 70 °C (cyan circles), after annealing at 90 °C (green circles) and after annealing to 115 °C (red circles).

exhibit Bragg rods, at a q_{xy} of 0.0147, which is consistent with particles that are 43 nm in diameter. Heating the sample to 70 °C results in intensification of the Bragg peaks and appearance of second order peaks, which indicates that longer-range ordering of the polymersomes is occurring and is consistent with the AFM data. Ordering of the particles suggests that the flattened polymersomes remain intact on the surface at temperatures of 70 °C and below. Heating the sample further from 90 to 120 °C results in the progressive loss of the Bragg rods, and, therefore, the registration between polymersomes is being lost. This result suggests that at temperatures above 90 °C that the structure of the polymersome is being destroyed, which again is in agreement with the observations from the AFM study.

2.4. Healing of Negatively Charged Rough Surfaces

The above experiments indicate that the polymersomes will adhere to negatively charged surfaces and that annealing leads to progressively smoother surfaces. We next sought to investigate the effect of treating an initially rough surface with the solution of polymersomes. The rough surface is intended to be a model for the roughness produced in features of patterned chemically amplified photoresists. The roughness inherent in the photolithographic processes is a major impediment to effective patterning below 32 nm. A method for preparation of surfaces that replicate the side walls of lithographically prepared features has been reported by Prabhu et al.[72] The method involves preparation of a polymeric film consisting of two layers, where the top layer consists of a $PtBMA_{0.44}$-*stat*-$MMA_{0.56}$ resist polymer that contains tertiary ester pendant groups and a PAG, while the bottom layer is an open-source extreme ultraviolet (EUV) resist polymer, which is based on polyhydroxystyrene chemistry (see Supporting Information, Figure S8),[73] and does not contain PAG. When exposed to UV light the PAG molecules in the upper layer undergo photodecomposition to yield a strong acid. The top layer acts as a feeder layer for photoacid, so that during the post-exposure bake step the photoacid diffuses into the bottom layer and catalytically deprotects the tertiary esters to yield carboxylic acids. The exposed film is then developed with an aqueous base solution (containing tetramethyl ammonium hydroxide, 2.38 wt%), so that the top layer and the regions to where the strong acid has diffused can be selectively dissolved, leaving behind the photoresist that has not undergone deprotection. In this method the strong acid undergoes random diffusion into the underlying polymer, analogous to the diffusion that occurs from exposed regions to unexposed regions during irradiation through a mask and subsequent post-exposure baking. This procedure creates roughness on a flat surface that is similar in magnitude and frequency to that observed on the side walls of conventional line-space patterns in photoresists.

The topology of the exposed rough surface was analyzed using AFM and a representative image is shown in **Figure 4**a. The RMS roughness was found to be 2.4 ± 0.5 nm, and is equivalent to approximately 7.2 nm when measured to 3σ, which is the industry standard for reporting of pattern roughness known as LER.[74] This value is of the same order of magnitude as LER values obtained from EUV lithography patterning.[75,76] This model rough surface was then dip coated with solutions of polymersomes and the AFM image after treatment is displayed in

Figure 4b. The morphology of the surface was observed to change after treatment with the polymersomes, where again spherical objects could be observed on the surface. The RMS roughness of this surface was found to be 2.2 ± 0.8 nm, which was not significantly different to that observed before coating. The surface coated with polymersomes was annealed at 70 °C, 90 °C, and 115 °C. The AFM height images at these three temperatures are shown in Figure 4c, d and e, respectively. As the annealing temperature was increased the spherical structures became less distinct and the RMS roughness values also decreased. For example, at 70 °C the RMS value was 1.0 ± 0.7 nm. However, further increases of the annealing temperature from 90 °C to 115 °C, resulted in values of RMS roughness that were not significantly different to that found at 70 °C as shown in Figure 4f, but the variance in roughness was observed to decrease. The control for this experiment was an untreated rough surface that was annealed to 115 °C and no significant change in the roughness was observed (see Supporting Information, Figure S11). This indicates that the roughness can be effectively reduced by as much as 70% once the treated surface is annealed at temperatures above T_g of the block copolymer, but in this case is below the T_g of the underlying resist, which was 123 °C. The AFM images also underwent PSD analysis to better understand how the PSD varies as a function of spatial frequency and the results are shown in Figure 4g. After deposition of the polymersomes a broad peak at 23 μm^{-1} could be observed and this corresponds to 43 nm, which is consistent with the diameter of the polymersomes when flattened on the surface. When the sample is heated to 70 °C the peak disappears and the PSD decreases slightly at spatial frequencies less than 20 μm^{-1}. Heating to 90 °C results in further decreases in PSD below 20 μm^{-1}, then heating to 115 °C results in a further decrease in the 10–20 μm^{-1}, while the PSD in other spatial frequencies remains unchanged. When the PSD spectra of the initial rough surface is compared to the sample annealed to 115 °C, it can be seen that there are significant decreases in PSD between 30–50 μm^{-1} and also at less than 4 μm^{-1}. Between 10–20 μm^{-1} the surface before treatment has slightly lower PSD values. However, the region that is most relevant to healing of roughness of patterned sidewalls is going to be in the 30–50 μm^{-1} which corresponds to 20–33 nm.

This strategy for healing roughness was also applied to resist features patterned by electron beam lithography, as shown in **Figure 5**a. The resist was patterned with line space patterns where the trenches have an average critical dimension (CD) of 174 ± 5 nm and a 3σ LER of 5.8 ± 0.4 nm. As a negative control, the pattern was annealed at 100 °C for 6 minutes, (see Figure 5b), after which the average CD was found to be 170 ± 2 nm and 3σ LER equal to 5.8 ± 0.4 nm. It was therefore confirmed that the annealing step did not significantly change the CD or LER (see Figure 5c). On the other hand, when the patterned resist was dip coated with the polymersome solution, the average CD of the trenches was found to decrease to 166 ± 1 nm and the 3σ LER was 5.7 ± 0.1 nm. The decrease the width of the trenches is attributed to the attachment of polymersomes to the side walls. (see Figure 5d). When the patterned resist was dip coated with the polymersome solution and annealed at 100 °C, (see Figure 5e) the average CD of the trenches was measured to be 160 ± 1 nm and 3σ LER was reduced to 3.4 ± 0.3 nm. This method shows a 58% decrease in the LER after treatment with the polymersomes followed by annealing step. Analysis of the LER using a PSD function suggests that the control samples, i.e. the patterned wafer, patterned and annealed wafer and patterned wafer treated with polymersomes (no annealing), did not exhibit any significant changes in LER (see **Figure 6**). On the other hand when the patterned wafer was treated with polymersomes and underwent annealing, healing of LER was observed in frequency ranges between 1 μm^{-1} (low frequency) and 100 μm^{-1} (high frequency).

The results presented above demonstrate that polymersomes composed of $PDMAEMA_{41}$-*block*-$PtBMA_{55}$ can be used to significantly smooth negatively charged rough surfaces (e.g., flat and patterned side-walls) in conjunction with a thermal annealing step. In the process described, the positively charged polymersomes electrostatically attach to the negatively charged surfaces. This is performed at room temperature where both polymers will be in a glassy state. Upon annealing at a temperature above

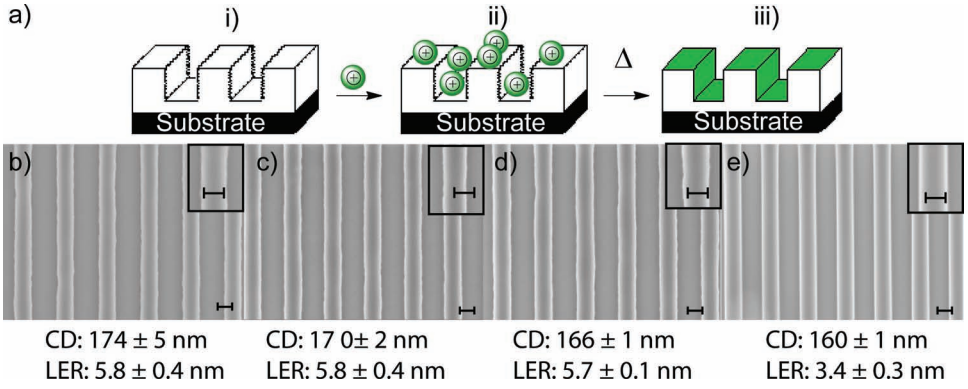

Figure 5. a) The process for healing the roughness of lithographically printed features. (i) represents a patterned photoresist, (ii) is after dip coating with a solution of polymersomes, and (iii) is after annealing at 100 °C. b) Top-down SEM micrographs of polyhydroxystyrene-based resist patterned using EB lithography. c) Patterned resist annealed at 100 °C as a negative control (i.e., the pattern has not been treated with polymersomes). d) Patterned after being treated with positively charged polymersomes without annealing. e) Patterned after being treated with positively charged polymersomes and annealing at 100 °C, where the roughness was found to decrease. For (b–e) the inset in the top right corner of each micrograph is a digitally magnified micrograph to better show the line roughness and extent of smoothing.

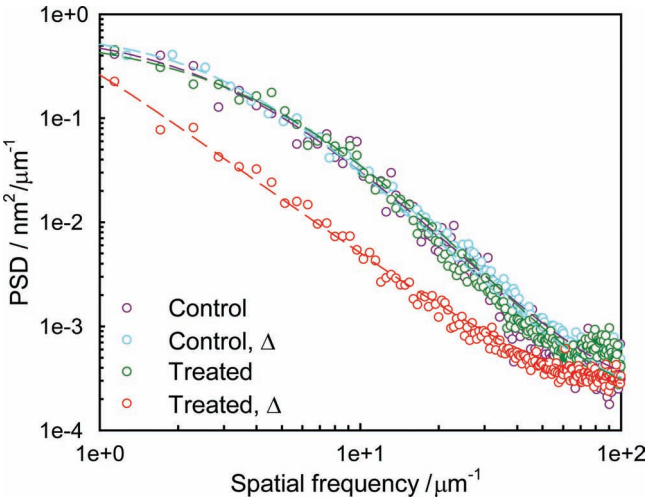

Figure 6. The PSD function determined for the patterned EUV resist and those further treated with polymersomes and/or thermal annealing (Δ). The patterned resists treated with both polymersomes and thermal annealing show a decrease in the low-frequency-range roughness. The control sample is a patterned resist prior to treatment and the control with heating is a patterned resist that was annealed in the absence of polymersomes. The treated sample is the patterned resist treated with polymersomes and the treated sample with heating is following annealing at 100 °C.

the T_g values of both blocks (but below that of the resist surface), the polymer chains in the block copolymer are free to undergo reorganization. The driving forces for the reorganization will depend on the relative energies of polymer at each of the interfaces. In this case the interface at the resist polymer surface is negatively charged and hydrophilic while the air interface is hydrophobic in comparison. Hence, it is expected that the PDMAEMA block will preferentially reside at the resist polymer surface and the hydrophobic PtBMA block will prefer to form an interface with air. It is proposed that the mechanism for the observed smoothing is then controlled by the balance of thermodynamic driving forces, which will tend toward the minimization of both the PDMEAMA/PtBMA and PtBMA/air interfacial area, balanced by the entropic penalties associated with the concomitant ordering of the PDMEAMA-*block*-PtBMA domains and stretching of the polymer chains in these domains. Hence, rather than simply conforming to the underlying roughness of the polymer resist the PtBMA chains at the air interface are able to adopt a smoother interface, which represents an overall decrease of the free energy.

3. Conclusions

We have reported a novel process for modulating the nanoscale roughness of both smooth and rough surfaces. The process involves the deposition of polymersomes formed from amphiphilic block copolymers and the controlled annealing of the coated films. It was shown that $PDMAEMA_{41}$-*block*-$PtBMA_{55}$ block copolymers with well defined compositions and molecular-weight distributions, prepared by RAFT polymerization, were able to self assemble into positively charged polymersomes at pH 6.3. When flat negatively charged surfaces were treated with solutions of the polymersomes it was possible to increase the roughness to an RMS value of 1.6 ± 0.6 nm, which could then be tuned down to 0.4 ± 0.2 nm by controlling the temperature of annealing. These results are likely to have significance in M/NEMS devices, where it can be necessary to tune the nanoscale roughness of surfaces to control the adhesion between two materials. Furthermore, when model rough surfaces were treated with the polymersomes and annealed, the surface roughness could be reduced by up to 70%. Application of this method to an e-beam patterned surface lead to a reduction in the LER value from 5.8 nm to 3.4 nm, a 58% decrease in the LER. The method proposed here provides a promising solution to reducing LER of nanoscale features that have been printed using photolithography, and has great potential to be used in semiconductor manufacture to improve pattern fidelity.

4. Experimental Section

Materials: 2-(*N*,*N*-dimethylamino) ethyl methacrylate (DMAEMA), 2-cyano-2-propyl benzodithioate (CPDB) (>97%), *tert*-butyl methacrylate (tBMA), methyl methacrylate (MMA), 2,2′-azobisisobutyronitrile (AIBN), glycidyl methacrylate (GMA), triphenylsulfonium triflate, 1,4-dioxane (anhydrous, 99.8%), trioctylamine (98%), propylene glycol monomethyl ether acetate (PGMEA) (99%), were all obtained from subsidiaries of Sigma–Aldrich. Aqueous 2.38% tetramethylammonium hydroxide (TMAH), was obtained from Tokyo OH CA KOGYO-Co CTP, the polyhydroxystyrene-based (PHOST-based) resist polymer solution (37 wt% in ethyl lactate) (622HSB-EL) was obtained from JSR Micro and pyrene was obtained from Koch Light Laboratories Ltd. AIBN was purified by recrystallization from methanol. The monomers were purified by passing through a basic alumina column immediately before use. All other chemicals were used as received.

Synthesis of PtBMA: tBMA (43.0 mmol), CPDB (0.72 mmol) and AIBN (3.6×10^{-2} mmol) were dissolved in 1,4-dioxane (4 mL). The solution was transferred to a Schlenk tube and was degassed by performing three consecutive freeze-vacuum-thaw cycles. Polymerization was carried out at 65 °C and was stopped at 56% conversion. The reaction was worked up by precipitating the polymer into a 90: 10 methanol: water mixture. A pink precipitate was obtained and dried under vacuum at 25 °C for 16 h. ^{1}H NMR (400 MHz, $CDCl_3$, δ): 2.1–1.8 (dd, 2H), 1.4 (s, 9H), and 1.1–1.0 (d, 3H). ^{13}C NMR (400 MHz, $CDCl_3$, δ): 177.4, 177.2, 176.7, 80.8, 46.4, 46.2, 29.6, 28.0, 27.8, 18.5, 17.8, 17.7. ATR-FTIR. ν = 2975, 2826, 2774, 1718, 1457, 1372, 1366, 1248, 1135 cm^{-1}. SEC (PSTY calibration): M_n = 6.6 kDa, $Đ_M$ = 1.1.

Synthesis of PDMAEMA-block-PtBMA: PtBMA (0.18 mmol), DMAEMA (7.8 mmol) and AIBN (3.6×10^{-2} mmol) were dissolved in 1,4-dioxane (2.8 mL). The solution was placed in a Schlenk tube and was degassed by performing three consecutive freeze-vacuum-thaw cycles before being flame sealed and immersed in a 65 °C oil bath. The crude PDMAEMA-*b*-PtBMA) at 56% conversion was precipitated in n-hexane as a pink precipitate, which was dried under vacuum at 25 °C overnight. ^{1}H NMR (400 MHz, $CDCl_3$, δ): 4.1 (s, 2H), 2.6 (s, 2H), 2.3 (s, 6H), 1.4 (s, 12H) and 1.0–0.8 (m, 6H). ^{13}C NMR (400 MHz, $CDCl_3$, δ): 177.7, 177.3, 176.7, 80.8, 63.0, 57.1, 45.8, 27.8, 18.5, 17.7, 16.6. SEC (triple detection): M_n = 15.3 kDa, $Đ_M$ = 1.1.

Synthesis of $PtBMA_{0.42}$-$PMMA0.56$-*stat*-$PGMA_{0.02}$: tBMA (20.0 mmol); MMA (34.1 mmol) GMA (27.0 mmol), AIBN (6.7×10^{-2} mmol), and CPDB (2.3×10^{-1} mmol) were mixed in a 20 mL vial and sealed with a Suba-Seal. The solution was degassed by purging with Ar for 15 min using a two needle approach. The polymerization was allowed to proceed at 60 °C overnight. The product was obtained by precipitating in n-hexane. A pink precipitate was obtained and this was dried under vacuum at 25 °C for 16 h. ^{1}H NMR (400 MHz, $CDCl_3$, δ): 3.59 (s, 3H),

3.49 (s, 1H), 2.8 (s, 1H), 2.6 (s, 1H) and 1.9–0.5 (17H). SEC (PSTY calibration): M_n = 9.6 kDa, $Đ_M$ = 1.1.

Preparation of a Negatively Charged Surface: Negatively charged surfaces were prepared by dissolving $PtBMA_{0.42}$-*stat*-$PMMA_{0.56}$-*stat*-$PGMA_{0.02}$ in propylene glycol monomethyl ether acetate (PGMEA) to give a 1.0 wt% solution along with triphenylsulfonium triflate, 5 wt% with respect to the polymer. The solution was spin-coated onto a silicon wafer (300 rpm/5 s, 3000 rpm/60 s) and was then baked on a hotplate at 120 °C for 1 min. The contact angle was determined to be 72.6 ± 2.6°, and the detail is shown in supporting information. To crosslink the film and deprotect the tertiary ester groups, the wafer was then exposed to UV (dose = 180 mJ/cm^2) followed by a baking step at 150 °C for 5 min. The film was rinsed with toluene and dried with a stream of nitrogen gas. The resulting film thickness was 19.8 ± 0.6 nm. Contact angle = 64.5 ± 2.4°.

Synthesis of $PtBMA_{0.44}$-stat-$PMMA_{0.56}$: tBMA (20 mmol), MMA (34 mmol), AIBN (6.7×10^{-2} mmol) and CPDB (0.23 mmol) were mixed in a 20 mL vial and sealed with a Suba-Seal. The solution was degassed by bubbling with Ar. The polymerization was allowed to proceed at 60 °C overnight. The product was obtained by precipitation in n-hexane. A pink precipitate was obtained and this was dried under vacuum at 25 °C. ^{1}H NMR (400 MHz, $CDCl_3$, δ): 3.59 (s, 3H) and 1.9–0.5 (16H). SEC (PSTY calibration): M_n = 20.4 kDa, $Đ_M$ = 1.24.

Preparation of the Polymersome Solution: A solution of $PDMAEMA_{41}$-*block*-$PtBMA_{55}$ (10 mg) with concentration of 1.2 mg/mL was prepared by dissolving the polymer in 0.75 mL of tetrahydrofuran (THF) and then with 18.2 MΩ cm Milli-Q water added drop-wise at a rate of 0.3 mL/min. THF was then removed under reduced pressure. The solution was diluted to 0.6 mg/mL and was adjusted to approximately pH 6.4 before use. The negatively charged surface and the rough surface were dipped coated in that solution, followed by washing with 18.2 MΩ cm Milli-Q water. The surfaces were dried at reduced pressure for 1 hour prior to AFM investigations. The annealing studies were carried out by heating the coated wafers at different temperatures for 6 minutes. The wafers then were studied by AFM.

Preparation of a PHOST-Based Model Surface that is Similar to Roughness Side Wall Features: The method used is an adaption from the work of Prabhu et al.[72] An open source EUV resist polymer, poly((4-hydroxystyrene)$_{0.6}$-*stat*-polystyrene$_{0.2}$-*stat*-$PtBMA_{0.2}$) (see Supporting Information, Figure S8) (10.0 wt%) was dissolved in PGMEA and trioctylamine (0.07 wt% with respect to the polymer), was also incorporated as the quencher. Note that this solution does not contain PAG. This solution was spin-coated onto a silicon wafer (300 rpm/5 s, 3000 rpm/60 s), which was followed by a post application bake (PAB) at 95 °C for 1 minute. The thickness of this layer was 90 ± 1 nm. Following this a solution of $PtBMA_{0.44}$-*stat*-$MMA_{0.56}$, 1.0 wt%, with 5.0 wt% triphenylsulfonium triflate with respect to the polymer, in anisole was spin-coated onto the PHOST-based coated Si wafer. (300 rpm/5 s, 4000 rpm/60 s), and this layer serves as a feeder layer of photoacid. At this stage, the thickness was measured to be 105 ± 3 nm. The water contact angle was 80 ± 2°. The bilayer film stack was irradiated with a UVA flood lamp to a dose of 180 mJ/cm^2. Irradiation was followed by a baking step at 105 °C for 30 s, development with 2.38% TMAH for 30 s and rinsing with 18.2 MΩ cm Milli-Q water. The final film thickness as determined by ellipsometry was 44 ± 4.9 nm and the water contact angle was 61 ± 3°.

Preparation of a Patterned PHOST-Based Surface: Firstly, silicon wafers were treated by piranha solution, followed by O_2 reactive ion etching at 200 W for 5 min. A resist solution was prepared by mixing an open source EUV resist polymer, poly((4-hydroxystyrene)$_{0.6}$-*stat*-polystyrene$_{0.2}$-*stat*-$PtBMA_{0.2}$) (see Supporting Information, Figure S8), 10 wt/v%, 5 wt/wt% of triphenylsulfonium triflate, with respect to the polymer and 0.05 wt/wt% of quencher (trioctyl amine) with respect to that polymer solution were dissolved in ethyl lactate. The solution was spin-coated at 4000 rpm for 60 s onto a silicon wafer, followed by a PAB on a hot plate at 95 °C for 60 s. The coated wafers were patterned using a Raith-150 electron-beam lithography (EBL) system manufactured by Raith GmbH. Specifically, the wafers were then exposed using an electron beam with an acceleration voltage of 10 keV, an aperture of 30 μm, a 6 mm working distance and with a beam current of 180 pA. Lithography patterns 10 mm long and 170 nm wide line were created in L-Edit Pro V.14 (Tanner EDA tool) and scanned at a dose of 15 μC/cm^2 with ten stitch fields of 100 μm by 100 μm in dimension. The samples were then baked at 105 °C for 60s on a hot plate followed by development in 2.38% TMAH for 30 s at room temperature, which was followed by rinsing with deionized water for 15 s and drying with a jet of N_2. Images of the patterned wafer were recorded multiple times before the wafer was cut into pieces, where one piece was used as a control group and the other pieces were treated with the solution of the polymersomes and annealed at 100 °C for 6 minutes. Images were examined by SEM at a magnification of 50 000 times at 2 keV with a working distance of 3 mm. The LER of the patterned features were analyzed using Summit v7.5.1, a commercial lithography metrology software package from EUV Technology (Martinez, CA). The LER was determined along the full length of the line using a polynomial edge detection algorithm with a threshold value of 0.5 determined by the average line threshold reference, and the associate frequency roughness were expressed as a power spectral density (PSD) function.

Characterization: Atomic force microscopy (AFM) was performed using a stand-alone MFP-3D instrument in tapping mode in air. The AFM was mounted on an antivibration table (Herzan LLC) and operated within an acoustic isolation enclosure (TMC). Height images were captured at 512 points per line at 0.8 Hz. Multi75DLC-50 cantilevers (75 ± 15 kHz, 3 N/m, and radius of curvature < 15 nm) were obtained from Budget Sensors and were used for the characterization of the surface topography. For cryo-TEM a 5 μL sample of the block copolymer solution was applied to a grid, blotted to a thin film with filter paper and immediately plunged into liquid ethane (–186 °C) in an FEI vitribot plunge-freezer. A cryoholder was used to transfer the grid containing the vitrified suspension into a Technai 12 TEM. The imaging was performed at 120 kV with low-dose procedures and magnifications of 69k. Zeta potential (ζ) measurements were determined by dynamic light scattering and laser Doppler electrophoresis (Zetasizer Nano ZS, Malvern Instruments, Worcestershire, UK). The surface tension measurements for determining the CAC of the polymersomes was assessed using a drop-shape analysis system (DSA 10). This allowed the interfacial tension between air and the block copolymer solution and thus the value of surface tension was able to be determined, which was done using the manufacturer's software. A SurPASS electrokinetic analyzer (Anton Paar) was used for surface zeta potential measurements. A SurPASS Clamping Cell was used to measure zeta potential of the silicon wafers. The sample was mounted between a spacer and the clamp. Grazing incidence small angle X-ray scattering (GISAXS) measurements were collected on the SAXS/WAXS beam-line at the Australian Synchrotron. The measurements were made with a sample-to-detector distance of 3.35 m and at photon energy of 12 keV. The beam was impinged onto the sample surface above the critical angle of the substrate. The sample exposure time was kept at five seconds. Data reported herein were obtained for an angle of incidence of 0.05°, which will results in surface sensitive spectra. The SXPS spectra were recorded on the soft X-ray beam line at the Australian Synchrotron. The synchrotron radiation was set to a photon energy of 650 eV. The electron analyzer pass energy was set to 10 eV. SXPS spectra were calibrated to the gold $4f_{7/2}$ peak (84 eV).

Supporting Information

Supporting Information is available from the Wiley Online Library or from the author.

Acknowledgements

This research was supported under the Australian Research Council (ARC) Linkage Projects Scheme (project number LP0989607), with Intel Corporation as the financial industry partner. I.B. and A.K.W. would also

like to acknowledge the ARC for a Future Fellowship (FT100100721) and Australian Professorial Fellowship, respectively. This work was performed in part at the Queensland node of the Australian National Fabrication Facility (ANFF), at the University of Queensland node of the Australian Microscopy and Microanalysis Research Facility (AMMRF) within the Centre of Microscopy and Microanalysis (CMM), and on the SAXS/WAXS and soft-X-ray beamlines at the Australian Synchrotron. Cryo-TEM images were collected with the assistance of Dr. Gary Morgan (CMM) and synchrotron measurements with the assistance of Drs. Nigel Kirby, Stephen Mudie, Adrian Hawley, and Bruce Cowie. The streaming potential data was collected in the Melbourne Centre for Nanofabrication (MCN) by Ms. Varsha V. Lal and Mr. Douglas Mair, the AFM measurements with the assistance of Dr. Elana Taran (ANFF-Q), and the SEM images were collected in the ANFF (ACT node) by Dr. Xijun Li. The authors thank Dr. Todd Younkin and Dr. Michael Leeson for valuable discussions.

Received: February 27, 2012
Revised: June 18, 2012
Published online: August 22, 2012

[1] H. Assender, V. Bliznyuk, K. Porfyrakis, *Science* **2002**, *297*, 973–976.
[2] M. Nosonovsky, B. Bhushan, *Adv. Funct. Mater.* **2008**, *18*, 843–855.
[3] S. N. Ramakrishna, L. Y. Clasohm, A. Rao, N. D. Spencer, *Langmuir* **2011**, *27*, 9972–9978.
[4] Z. Burton, B. Bhushan, *Nano Lett.* **2005**, *5*, 1607–1613.
[5] V. A. Ganesh, H. K. Raut, A. S. Nair, S. Ramakrishna, *J. Mater. Chem.* **2011**, *21*, 16304-16322.
[6] G. Jin, H. Jeon, G. Kim, *Soft Matter* **2011**, *7*, 4723–4728.
[7] G. Wei, P. X. Ma, *Adv. Funct. Mater.* **2008**, *18*, 3568–3582.
[8] H. Ma, J. Hu, P. X. Ma, *Adv. Funct. Mater.* **2010**, *20*, 2833–2841.
[9] M. D. Kofron, A. Griswold, S. G. Kumbar, K. Martin, X. Wen, C. T. Laurencin, *Adv. Funct. Mater.* **2009**, *19*, 1351–1359.
[10] Y. Zhu, A. Wang, W. Shen, S. Patel, R. Zhang, W. L. Young, S. Li, *Adv. Funct. Mater.* **2010**, *20*, 1433–1440.
[11] D. J. Stickler, N. S. Morris, R. J. C. McLean, C. Fuqua, *Appl. Environ. Microbiol.* **1998**, *64*, 3486–3490.
[12] R. Maboudian, *J. Vac. Sci. Technol. B* **1997**, *15*, 20.
[13] F. W. DelRio, M. P. de Boer, J. A. Knapp, E. David Reedy, P. J. Clews, M. L. Dunn, *Nat. Mater.* **2005**, *4*, 629–634.
[14] Y. Ban, S. Sundareswaran, D. Z. Pan, *J. Micro/Nanolithogr. MEMS MOEMS* **2010**, *9*, 041206.
[15] C. Gustin, L. H. A. Leunissen, A. Mercha, S. Decoutere, G. Lorusso, *Thin Solid Films* **2008**, *516*, 3690–3696.
[16] B. Wu, A. Kumar, *J. Vac. Sci. Technol., B* **2007**, *25*, 1743–1761.
[17] W. Steinhögl, G. Schindler, G. Steinlesberger, M. Traving, M. Engelhardt, *Microelectron. Eng.* **2004**, *76*, 126–130.
[18] M. Stucchi, M. Bamal, K. Maex, *Microelectron. Eng.* **2007**, *84*, 2733–2737.
[19] K. Hyun-Woo, L. Ji-Young, J. Shin, W. Sang-Gyun, C. Han-Ku, M. Joo-Tae, *IEEE Trans. Electron Dev.* **2004**, *51*, 1984–1988.
[20] A. Asenov, S. Kaya, A. R. Brown, *IEEE Trans. Electron Dev.* **2003**, *50*, 1254–1260.
[21] A. Yu, H. Liu, J. P. Blinco, K. S. Jack, M. Leeson, T. R. Younkin, A. K. Whittaker, I. Blakey, *Macromol. Rapid Commun.* **2010**, *31*, 1449–1455.
[22] P. P. Naulleau, D. Niakoula, G. J. Zhang, *J. Vac. Sci. Technol. B* **2008**, *26*, 1289–1293.
[23] I. W. Cho, H. Kim, J. H. You, H. K. Oh, *Jpn. J. Appl. Phys.* **2010**, *49*, 041206.
[24] L. Chen, Y.-K. Goh, K. Lawrie, Y. Chuang, E. Piscani, P. Zimmerman, I. Blakey, A. K. Whittaker, *Radiat. Phys. Chem.* **2011**, *80*, 242–247.
[25] K. J. Lawrie, I. Blakey, J. P. Blinco, H. H. Cheng, R. Gronheid, K. S. Jack, I. Pollentier, M. J. Leeson, T. R. Younkin, A. K. Whittaker, *J. Mater. Chem.* **2011**, *21*, 5629–5637.
[26] K. Lawrie, I. Blakey, J. Blinco, R. Gronheid, K. Jack, I. Pollentier, M. J. Leeson, T. R. Younkin, A. K. Whittaker, *Radiat. Phys. Chem.* **2011**, *80*, 236–241.
[27] M. D. Rodwogin, C. S. Spanjers, C. Leighton, M. A. Hillmyer, *ACS Nano* **2010**, *4*, 725–732.
[28] C. Tang, S.-M. Hur, B. C. Stahl, K. Sivanandan, M. Dimitriou, E. Pressly, G. H. Fredrickson, E. J. Kramer, C. J. Hawker, *Macromolecules* **2010**, *43*, 2880–2889.
[29] A. Baruth, M. D. Rodwogin, A. Shankar, M. J. Erickson, M. A. Hillmyer, C. Leighton, *ACS Appl. Mater. Interfaces* **2011**, *3*, 3472–3481.
[30] J. G. Son, J.-B. Chang, K. K. Berggren, C. A. Ross, *Nano Lett.* **2011**,*11*, 5079–5084.
[31] I. Bita, J. K. W. Yang, Y. S. Jung, C. A. Ross, E. L. Thomas, K. K. Berggren, *Science* **2008**, *321*, 939–943.
[32] R. Ruiz, H. Kang, F. A. Detcheverry, E. Dobisz, D. S. Kercher, T. R. Albrecht, J. J. de Pablo, P. F. Nealey, *Science* **2008**, *321*, 936–939.
[33] C. T. Black, R. Ruiz, G. Breyta, J. Y. Cheng, M. E. Colburn, K. W. Guarini, H. C. Kim, Y. Zhang, *IBM J. Res. Dev.* **2007**, *51*, 605–633.
[34] J. Y. Cheng, C. A. Ross, H. I. Smith, E. L. Thomas, *Adv. Mater.* **2006**, *18*, 2505–2521.
[35] M. P. Stoykovich, H. Kang, K. C. Daoulas, G. Liu, C.-C. Liu, J. J. de Pablo, M. Mueller, P. F. Nealey, *ACS Nano* **2007**, *1*, 168–175.
[36] J. K. Bosworth, M. Y. Paik, R. Ruiz, E. L. Schwartz, J. Q. Huang, A. W. Ko, D.-M. Smilgies, C. T. Black, C. K. Ober, *ACS Nano* **2008**, *2*, 1396–1402.
[37] Y. Tada, S. Akasaka, H. Yoshida, H. Hasegawa, E. Dobisz, D. Kercher, M. Takenaka, *Macromolecules* **2008**, *41*, 9267–9276.
[38] S.-J. Jeong, H.-S. Moon, B. H. Kim, J. Y. Kim, J. Yu, S. Lee, M. G. Lee, H. Choi, S. O. Kim, *ACS Nano* **2010**, *4*, 5181–5186.
[39] J. G. Son, A. F. Hannon, K. W. Gotrik, A. Alexander-Katz, C. A. Ross, *Adv. Mater.* **2011**, *23*, 634–639.
[40] H.-H. Cheng, I. Keen, A. Yu, Y.-M. Chuang, I. Blakey, K. S. Jack, M. J. Leeson, T. R. Younkin, A. K. Whittaker, *Proc. SPIE* **2011**, *7970*, 79701V.
[41] J. W. Jeong, W. I. Park, M.-J. Kim, C. A. Ross, Y. S. Jung, *Nano Lett.* **2011**, *11*, 4095–4101.
[42] S.-M. Park, X. Liang, B. D. Harteneck, T. E. Pick, N. Hiroshiba, Y. Wu, B. A. Helms, D. L. Olynick, *ACS Nano* **2011**, *5*, 8523–8531.
[43] S.-J. Jeong, H.-S. Moon, J. Shin, B. H. Kim, D. O. Shin, J. Y. Kim, Y.-H. Lee, J. U. Kim, S. O. Kim, *Nano Lett.* **2010**, *10*, 3500–3505.
[44] S.-J. Jeong, J. E. Kim, H.-S. Moon, B. H. Kim, S. M. Kim, J. B. Kim, S. O. Kim, *Nano Lett.* **2009**, *9*, 2300–2305.
[45] B. H. Kim, D. H. Lee, J. Y. Kim, D. O. Shin, H. Y. Jeong, S. Hong, J. M. Yun, C. M. Koo, H. Lee, S. O. Kim, *Adv. Mater.* **2011**, *23*, 5618–5622.
[46] S. H. Park, D. O. Shin, B. H. Kim, D. K. Yoon, K. Kim, S. Y. Lee, S.-H. Oh, S.-W. Choi, S. C. Jeon, S. O. Kim, *Soft Matter* **2010**, *6*, 120–125.
[47] J. Y. Cheng, C. T. Rettner, D. P. Sanders, H.-C. Kim, W. D. Hinsberg, *Adv. Mater.* **2008**, *20*, 3155–3158.
[48] J. Y. Cheng, D. P. Sanders, H. D. Truong, S. Harrer, A. Friz, S. Holmes, M. Colburn, W. D. Hinsberg, *ACS Nano* **2010**, *4*, 4815–4823.
[49] J. Chiefari, Y. K. Chong, F. Ercole, J. Krstina, J. Jeffery, T. P. T. Le, R. T. A. Mayadunne, G. F. Meijs, C. L. Moad, G. Moad, E. Rizzardo, S. H. Thang, *Macromolecules* **1998**, *31*, 5559–5562.
[50] G. Moad, E. Rizzardo, S. H. Thang, *Aust. J. Chem* **2006**, *59*, 699–692.
[51] C. Barner-Kowollik, T. P. Davis, J. P. A. Heuts, M. H. Stenzel, P. Vana, M. Whittaker, *J. Polym. Sci., Part A: Polym. Chem.* **2003**, *41*, 365–375.
[52] J. Bernard, X. Hao, T. P. Davis, C. Barner-Kowollik, M. H. Stenzel, *Biomacromolecules* **2006**, *7*, 232–238.
[53] Z. Merican, T. L. Schiller, C. J. Hawker, P. M. Fredericks, I. Blakey, *Langmuir* **2007**, *23*, 10539–10545.

[54] R. Plummer, D. J. T. Hill, A. K. Whittaker, *Macromolecules* **2006**, *39*, 8379–8388.
[55] B. Liu, A. Kazlauciunas, J. T. Guthrie, S. Perrier, *Macromolecules* **2005**, *38*, 2131–2136.
[56] K. J. Thurecht, I. Blakey, H. Peng, O. Squires, S. Hsu, C. Alexander, A. K. Whittaker, *J. Am. Chem. Soc.* **2010**, *132*, 5336–5337.
[57] G. Moad, E. Rizzardo, S. H. Thang, *Aust. J. Chem.* **2009**, *62*, 1402–1472.
[58] C. S. Patrickios, W. R. Hertler, N. L. Abbott, T. A. Hatton, *Macromolecules* **1994**, *27*, 930–937.
[59] D. Fournier, R. Hoogenboom, H. M. L. Thijs, R. M. Paulus, U. S. Schubert, *Macromolecules* **2007**, *40*, 915–920.
[60] M. J. Bruining, H. G.T. Blaauwgeers, R. Kuijer, P. Elisabeth, R. M. M. A. Nuijts, L. H. Koole, *Biomaterials* **2000**, *21*, 595–604.
[61] H. Suzuki, T. Miyamoto, *Macromolecules* **1990**, *23*, 1877–1879.
[62] A. Blanazs, S. P. Armes, A. J. Ryan, *Macromol. Rapid Commun.* **2009**, *30*, 267–277.
[63] S. Piogé, L. Fontaine, C. d. Gaillard, E. Nicol, S. Pascual, *Macromolecules* **2009**, *42*, 4262–4272.
[64] D. P. Sanders, *Chem. Rev.* **2010**, *110*, 321–360.
[65] J. W. Thackeray, *J. Micro/Nanolithogr. MEMS MOEMS* **2011**, *10*, 033009.
[66] J. H. Hah, S. Mayya, M. Hata, Y. K. Jang, H. W. Kim, M. Ryoo, S. G. Woo, H. K. Cho, J. T. Moon, *J. Vac. Sci. Technol. B* **2006**, *24*, 2209–2213.
[67] S. L. Walker, S. Bhattacharjee, E. M. V. Hoek, M. Elimelech, *Langmuir* **2002**, *18*, 2193–2198.
[68] E. Han, I. In, S.-M. Park, Y.-H. La, Y. Wang, P. F. Nealey, P. Gopalan, *Adv. Mater.* **2007**, *19*, 4448–4452.
[69] D. Y. Ryu, K. Shin, E. Drockenmuller, C. J. Hawker, T. P. Russell, *Science* **2005**, *308*, 236–239.
[70] P. M. Dietrich, N. Graf, T. Gross, A. Lippitz, S. Krakert, B. Schüpbach, A. Terfort, W. E. S. Unger, *Surf. Interface Anal.* **2010**, *42*, 1184–1187.
[71] N. Matsukawa, K. Nishio, K. Sano, K. Shiba, I. Yamashita, *Langmuir* **2009**, *25*, 3327–3330.
[72] V. M. Prabhu, S. Kang, D. L. VanderHart, S. K. Satija, E. K. Lin, W.-L. Wu, *Adv. Mater.* **2010**, 388–408.
[73] H. Xu, J. M. Blackwell, T. R. Younkin, K. Min, *Proc. SPIE* **2009**, *7273*, 72731J.
[74] H. B. Cao, J. M. Roberts, J. Dalin, M. Chandhok, R. P. Meagley, E. M. Panning, M. K. Shell, B. J. Rice, *Proc. SPIE* **2003**, *5039*, 484–491.
[75] P. P. Naulleau, C. Rammeloo, J. P. Cain, K. Dean, P. Denham, K. A. Goldberg, B. Hoef, B. L. Fontaine, A. R. Pawloski, C. Larson, G. Wallraff, *Proc. SPIE* **2006**, *6151*, 61510Y.
[76] L. Chen, Y. K. Goh, H. H. Cheng, B. W. Smith, P. Xie, W. Montgomery, A. K. Whittaker, I. Blakey, *J. Polym. Sci., Part A: Polym. Chem.* **2012**, *DOI: 10.1002/pola.26232*.